SUPPORTING INFORMATION

Designed, Helical Protein Nanotubes with Variable Diameters from a Single Building Block

Jeffrey D. Brodin[†‡], Sarah J. Smith[‡], Jessica R. Carr, F. Akif Tezcan*

Department of Chemistry and Biochemistry, University of California, San Diego, 9500 Gilman Drive, La Jolla, CA 92093-0356

Supporting Materials and Methods

Site-directed mutagenesis and protein expression/purification

The R59H and T96C amino acid substitutions were introduced into the pET-ridc3[1] expression vector using QuikChange (Stratagene) site-directed mutagenesis and primers obtained from Integrated DNA technologies. The resulting plasmid, pET-^{H59C96}ridc3, was transformed into chemically competent E. Coli cells and expressed and purified as previously reported.[2] The molecular weight of the purified protein was determined by matrix assisted laser desorption/ionization time of flight mass spectrometry (MALDI-TOF MS) to verify the incorporation of the R59H and T96C amino acid substitutions (calculated mass = 24410 Da, observed mass = 24415 Da; Fig. S2a). The purity of ^{H59C96}RIDC3 and formation of the disulfide-linked dimer, ^{H59C96}RIDC3$_2$ (R_2), were confirmed by SDS-PAGE (Fig. S2b).

Macromolecular crystallography

Single crystals of Zn_8R_4 were obtained via Zn-directed assembly in bulk solutions containing 50 μM R_2, 100 mM TRIS (pH 7.5) and 2.5 mM $ZnCl_2$. After the addition of $ZnCl_2$, the solutions immediately became turbid and a red precipitate collected at the bottom of the solution over the course of ~ 1 wk. A 20-μL aliquot of the resuspended precipitate was deposited onto a glass slide and imaged by light microscopy, which revealed the presence of hexagonal crystals (Fig. S3).

Crystals suitable for diffraction experiments were transferred to a solution of mother liquor containing 20% glycerol as the cryoprotectant and flash-frozen in liquid nitrogen. X-ray diffraction data were collected at 100 K at SSRL BL12-2 and subsequently integrated using MOSFLM and scaled with SCALA.[3] Structures were then determined by molecular replacement using PHASER[4] and subjected to rigid-body, positional and thermal refinement in REFMAC,[5] along with manual rebuilding in COOT.[6] Crystallographic data collection and refinement statistics are listed in Table S1. All figures of the resulting structures were produced using PYMOL.[7]

Assembly of Zn_8R_4 nanostructures

Zn_8R_4 nanostructures were assembled in 200 µL solutions containing 50 µM R_2 and the indicated buffer. $ZnCl_2$ was added to these solutions from a 40 mM stock solution to obtain the indicated R_2:Zn^{II} ratios. After the addition of $ZnCl_2$, the solutions rapidly became turbid and the protein gradually sedimented over the course of ~1 wk. Small aliquots of the resuspended precipitate were removed at the indicated time points and analyzed by negative stain or cyroEM.

Preparation of specimens and imaging of Zn_8R_4 nanostructures

A 2-µL aliquot of a solution containing the indicated Zn_8R_4 nanostructures was drop cast onto a carbon coated Cu-mesh grid that had been made hydrophilic by glow discharge. After allowing the sample to adhere to the carbon support for 1 min., excess fluid was removed by blotting with Whatman filter paper. The sample was then washed with deionized water (18 mΩ) and stained with 2% uranyl acetate. Grids were imaged on an FEI Sphera transmission electron microscope equipped with an LaB_6 electron gun operated at 200 keV. Images of the negatively stained specimens were recorded on a Gatan 2K2 CCD using objective-lens underfocus settings that ranged from 800 to 1200 nm.

Samples were prepared for cyro-EM samples by drop casting a 3.5-µl aliquot of the indicated sample onto a homemade lacey carbon grid that had been made hydrophilic by glow discharge. The sample was incubated on the grid for approximately 1 min and was then blotted for 8 s using Whatman filter paper before being plunged into liquid ethane. The samples were then stored under liquid nitrogen until analysis on a FEI 200 Sphera electron microscope operated at an accelerating voltage of 200 keV. Images were recorded on a Gatan 2K2 CCD using objective-lens underfocus settings that ranged from 1 to 3 μm.

Processing of TEM micrographs

All image processing was performed using the 2DX software package.[8] A mask was applied around individual nanostructures (planar arrays or 1D nanotubes) using the “mask crystal from polygon” function. Fast Fourier transforms (FFTs) of the masked regions were then generated using the “calculate FFT” function. Individual reflections visible in calculated FFTs were selected and served as the basis for determining lattice parameters for each nanostructure using the “evaluate lattice” function. Images were then Fourier-filtered and unbent using the “Unbend 1” and “Unbend 2” functions.

Calculation of persistence length

The persistence lengths of Type I, II and II nanotubes were calculated using FiberApp.[9] Tubes were selected for analysis if they did not cross other tubes and if their entire length was visible in a single image. The persistence length of at least 75 individual tubes from each class and method of analysis (negative stained or cryoEM) were calculated using the MS End-to-end Distance (MSED) module. FiberApp was used to trace each fiber selected for analysis. MSED fitting analysis was performed over the full range of length values using the equation

$$\langle R^2 \rangle = 4\lambda[l - 2\lambda(1 - e^{-l/2\lambda})]$$

where λ is the persistence length, R is the end to end distance between two points, and l is the contour length of the nanotube. A processing length was chosen by determining where the error in fitting was lowest, and this value was used for each of the calculations (fits are shown in Fig. S14). The persistence length was then used to calculate Young's modulus using equation 1.

Table S1. X-ray data collection and refinement statistics for *Zn_8R_4*.

*denotes highest resolution shell

Data collection location	SSRL BL 12-2
Unit cell dimensions (Å)	52.9 × 52.9 × 257.1 α=γ=90°, β=120°
Space group	$P6_122$
Resolution (Å)	85.69 – 2.46
X-ray Energy (keV)	12,657
Number unique reflections	8104
Redundancy	3.5
Completeness (%)*	95.1 (87.7)
<I/σI>*	6.7 (3.4)
R_{symm} (%)*	8.6 (21.9)
R_{work}/R_{free} (%)	22.5/29.2
R.m.s. deviations	
Bond lengths (Å)	0.011
Bond angles (°)	1.385
Ramachandran plot (%)	
Most favored	99
Allowed	1
Disallowed	0.0

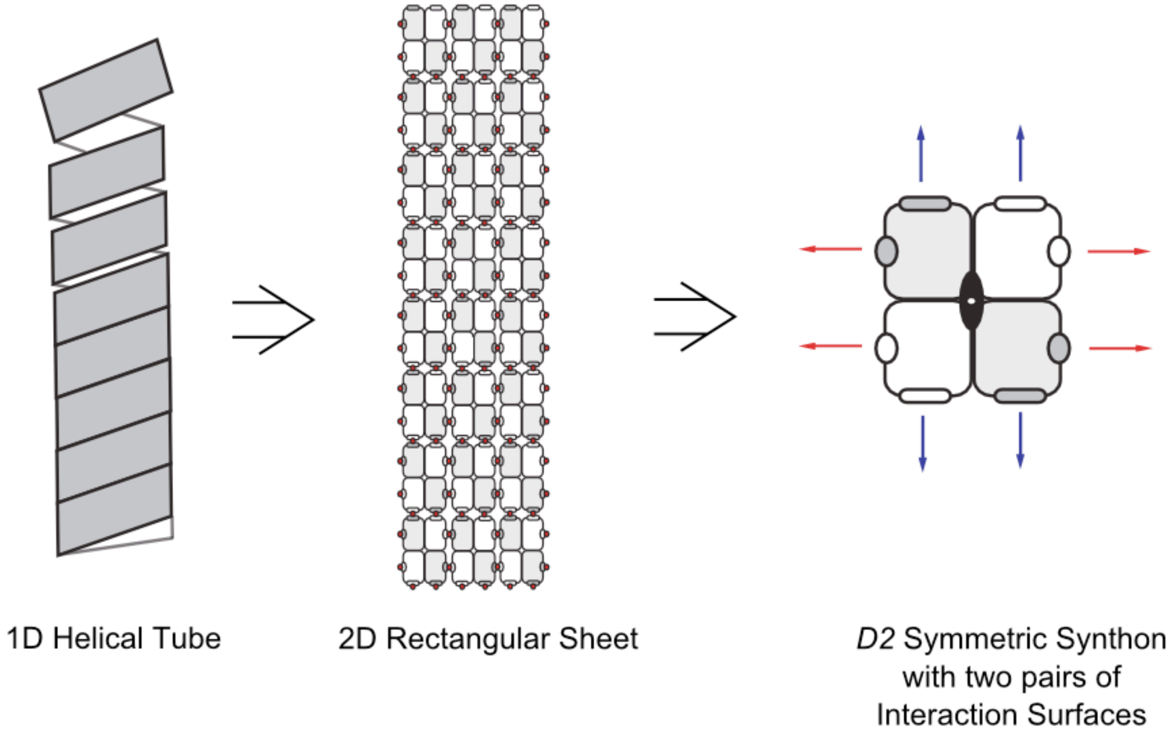

Figure S1. Retrosynthetic analysis of a 2D helical nanotube**.** Individual nanotubes (left) are formed by the folding of an anisotropic 2D array (center) that is composed of individual D_2 symmetric synthons (right). The formation of an anisotropic array is driven by the presence of bidirectional interaction motifs that have differential binding strengths.

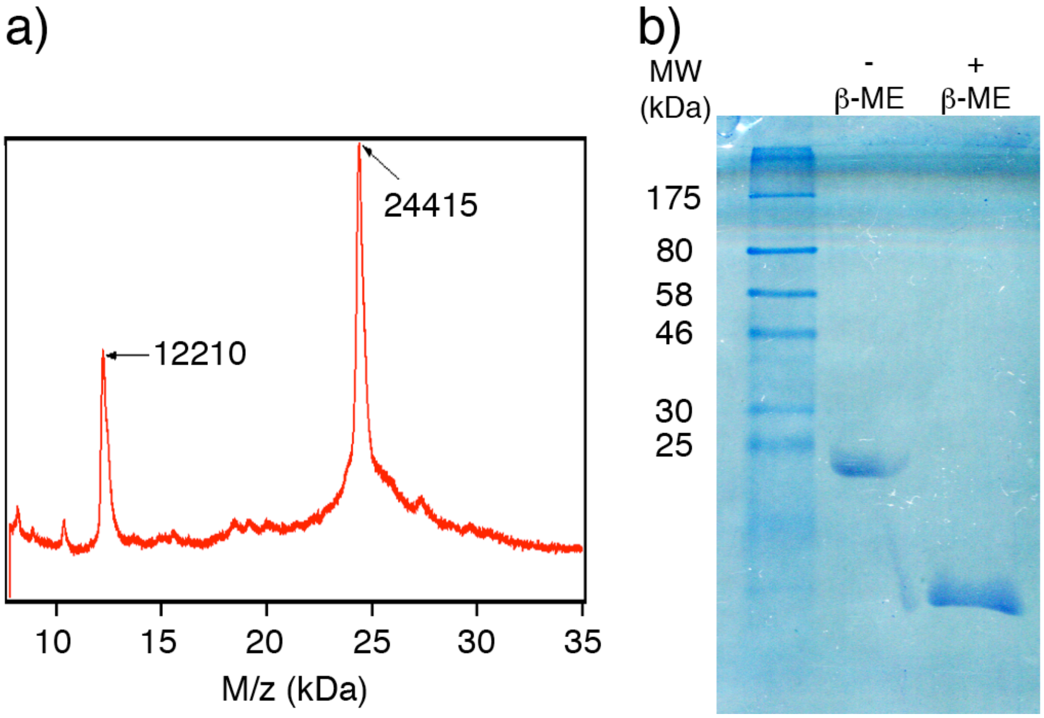

Figure S2. Characterization of disulfide-crosslinked R_2. (a) MALDI mass spectrum of R_2. (b) SDS PAGE gel of R_2 after denaturation in loading buffer with (right line) or without (center lane) β-mercaptoethanol (β-ME). In the presence of β-ME, the C96-C96 bond is reduced, yielding the monomeric species

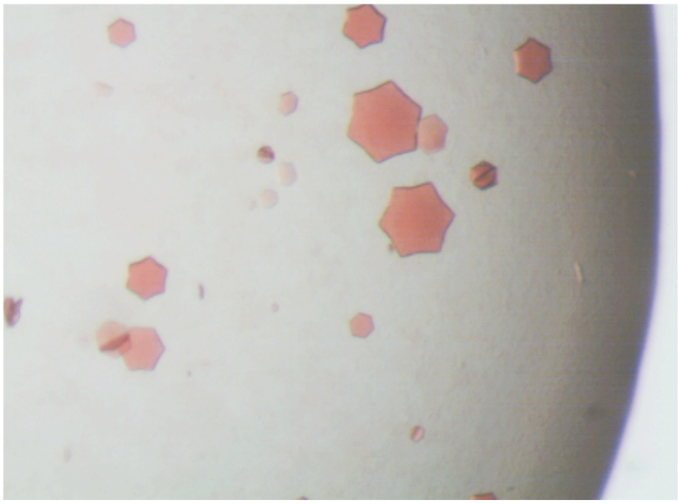

Figure S3. Light micrograph of Zn_8R_4 crystals obtained via Zn-directed assembly.

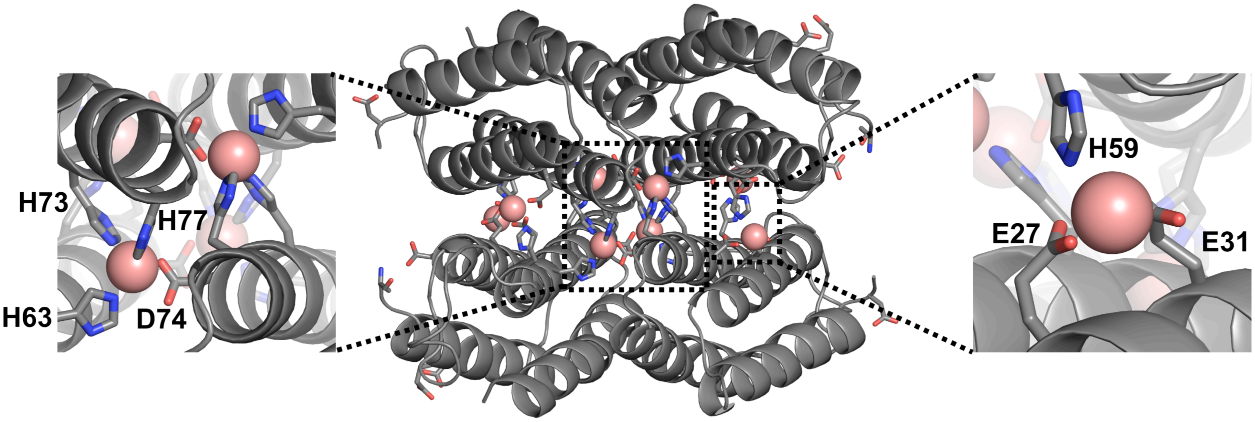

Figure S4. Internal Zn^{II} coordination sites to form Zn_8R_4 from R_2.

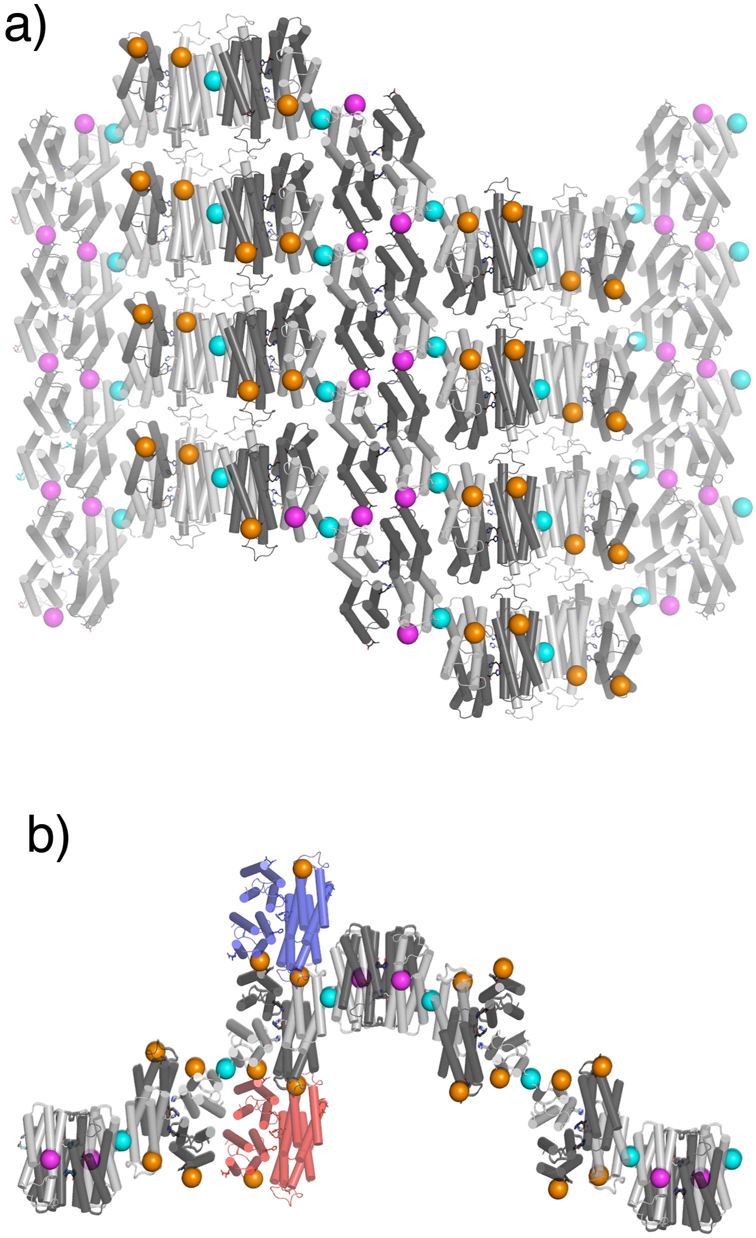

Figure S5. Mechanism for stacking of 2D Zn_8R_4 arrays into 3D crystals. (a) Cartoon depiction of a crystallographically characterized 2D Zn-mediated array. 2D arrays are stabilized by Zn ions coordinated by N-terminal and tetracarboxylate coordination motifs, which are shown as magenta and cyan spheres, respectively. N-terminal coordination sites that are oriented perpendicular to the 2D array (orange spheres) allow for the growth of 3D crystals or multi-walled nanotubes. (b) Front view of a Zn-mediated 2D array. The blue and red tetramers are coordinated to Zn^{II} sites in front of and behind the 2D array, respectively.

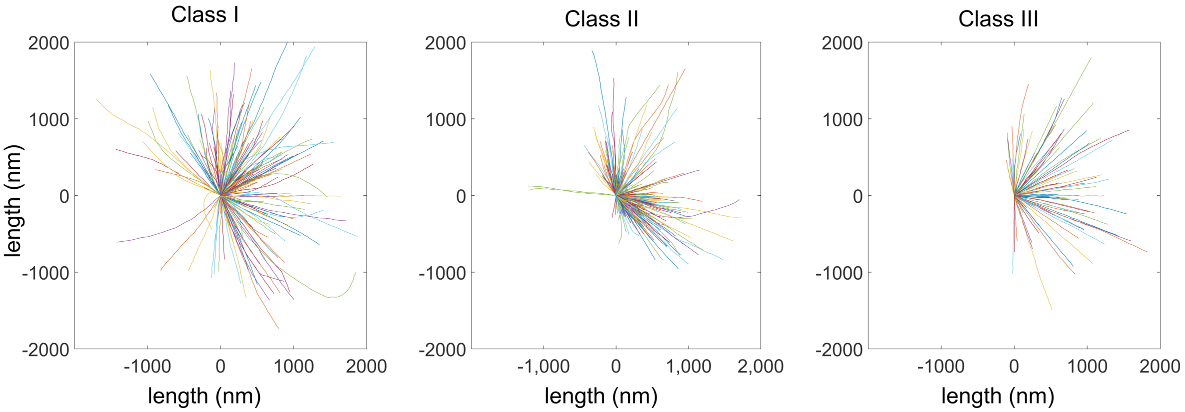

Figure S6. Traces of individual nanotubes used for determining the parameters listed in Table 1. Each tube was traced using the FiberApp program, and the initial coordinates were placed at (0,0) so that each tube extends from the center of the plot.

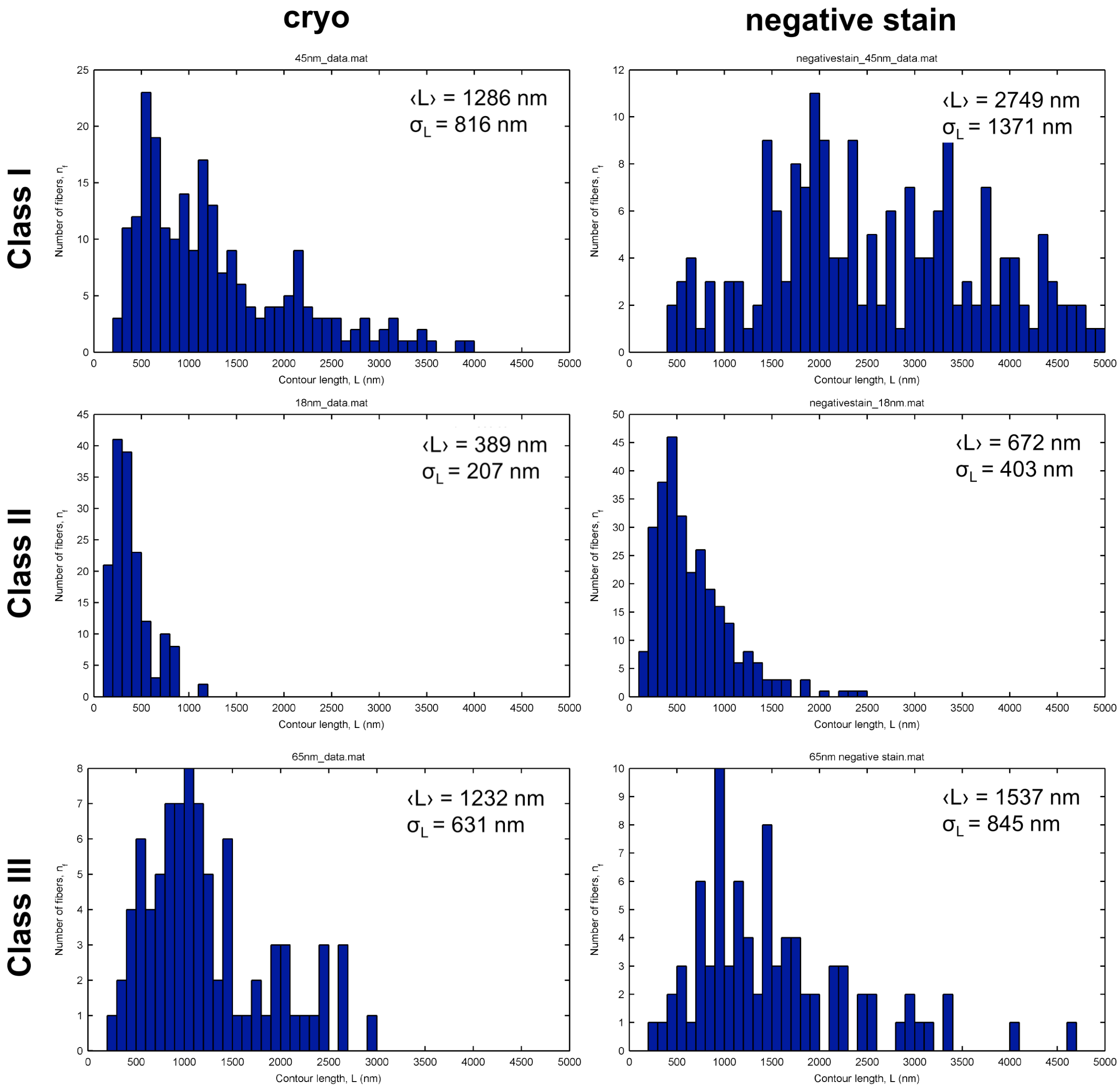

Figure S7. Contour length distributions of each class of nanotubes.

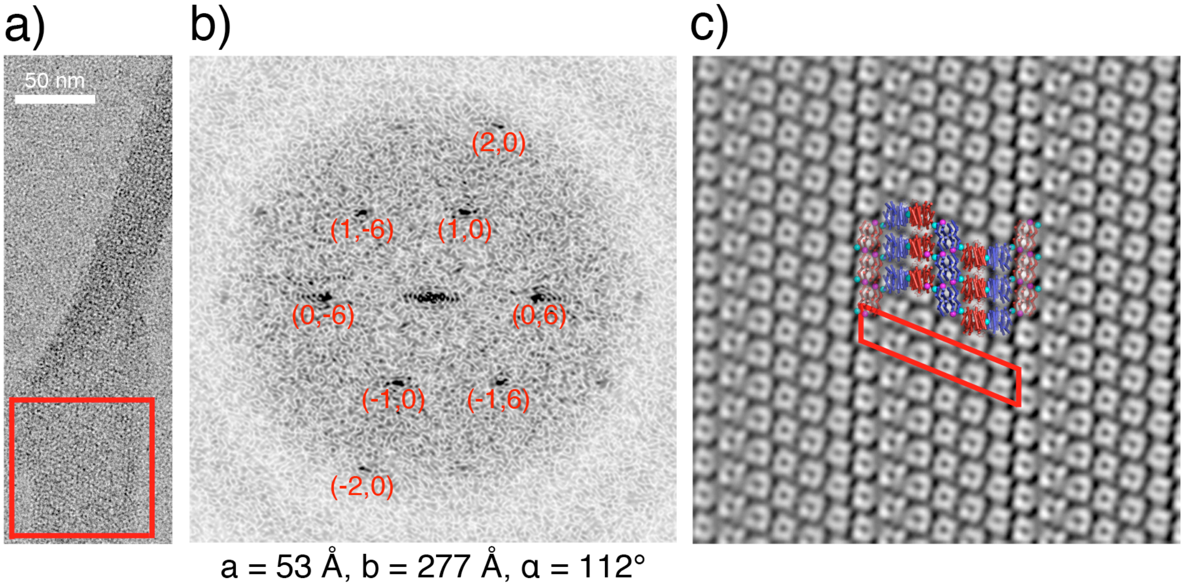

Figure S8. TEM micrograph (a), calculated Fourier transform (b) and Fourier-filtered image (c) of the planar region of a Class I nanotube.

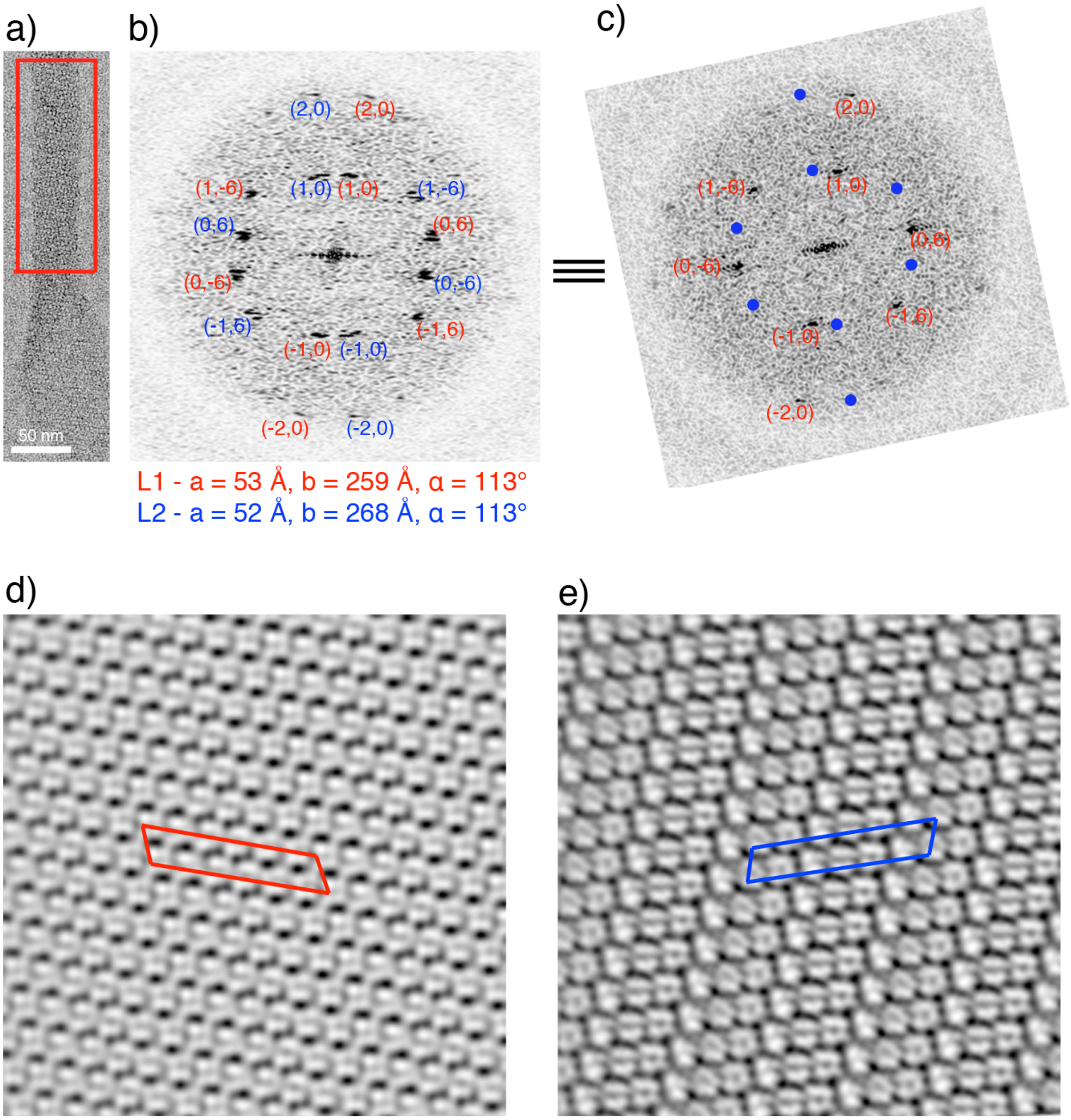

Figure S9. Image processing of the tubular region of a Class I nanotube. (a) Image of single Zn_8R_4 nanotube. (b) Fourier transform of boxed region of the nanotube highlighting the lattices from the top and bottom of a flattened tube. (c) Fourier transform of the flattened region of a single tube rotated 7° to account for the angle each tube makes with the meridian. Blue dots represent a theoretical lattice generated by inserting a mirror plane along the tube meridian. (d and e) 2D reconstructions of each lattice in (b).

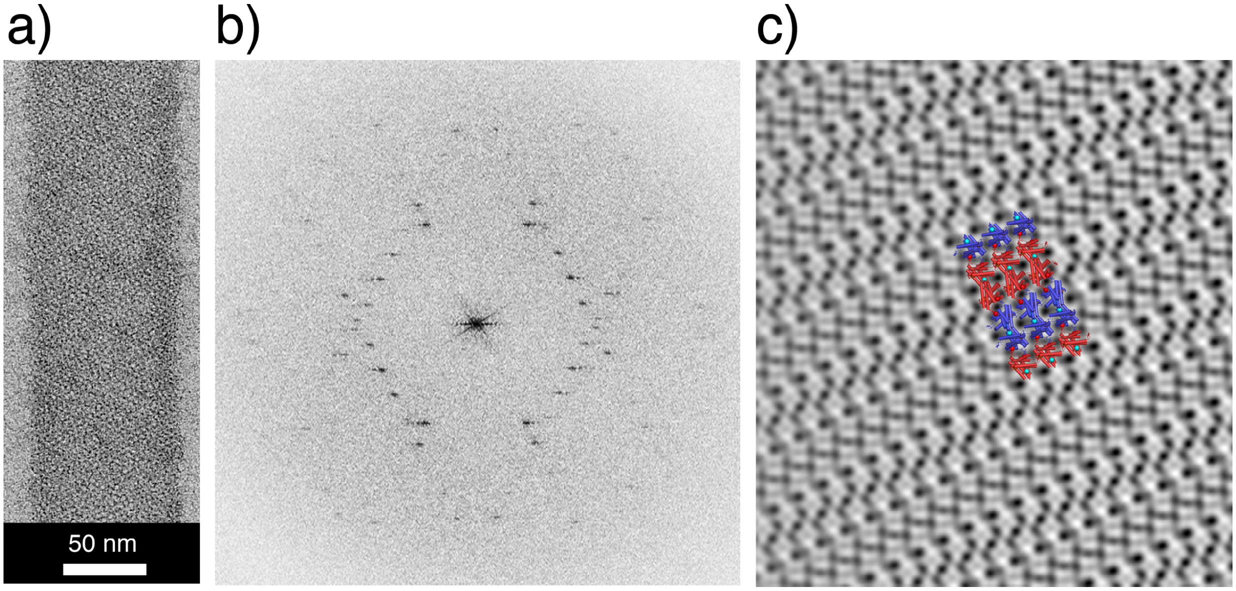

Figure S10. (a) TEM micrograph, (b) calculated Fourier transform, and (c) Fourier-filtered image of a single Zn-RIDC3 nanotube. The diameters of Zn-RIDC3 nanotubes were significantly wider (~90 nm) than those obtained with Zn_8R_4. Additionally, the structural units are clearly distinct from those of Zn_8R_4 nanotubes and are composed of dimeric subunits that assemble into open, C-shaped tetramers (blue or red cartoons) with orientations that alternate along the circumference of the nanotube.

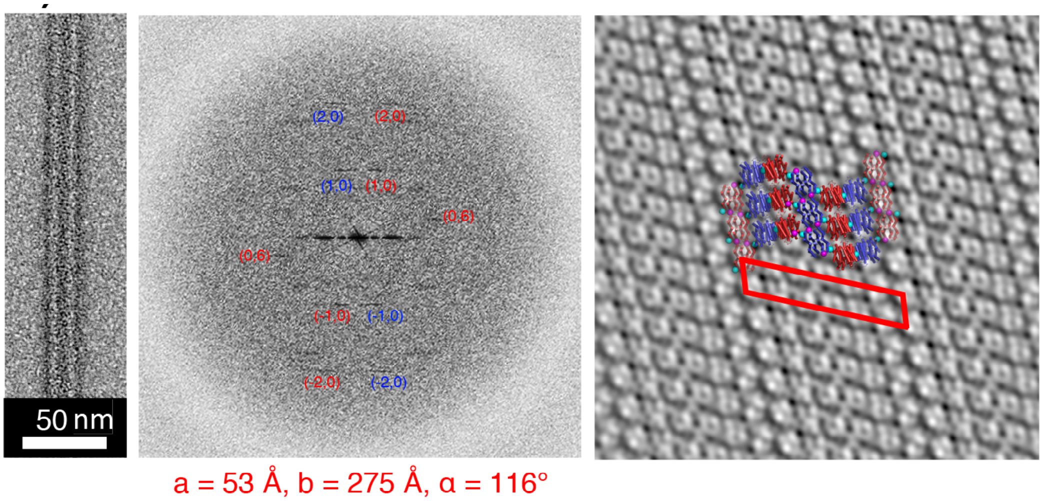

Figure S11. TEM images of a single nanotube (left), indexed Fourier transform (center), and 2D reconstruction (right) of a Class II nanotube.

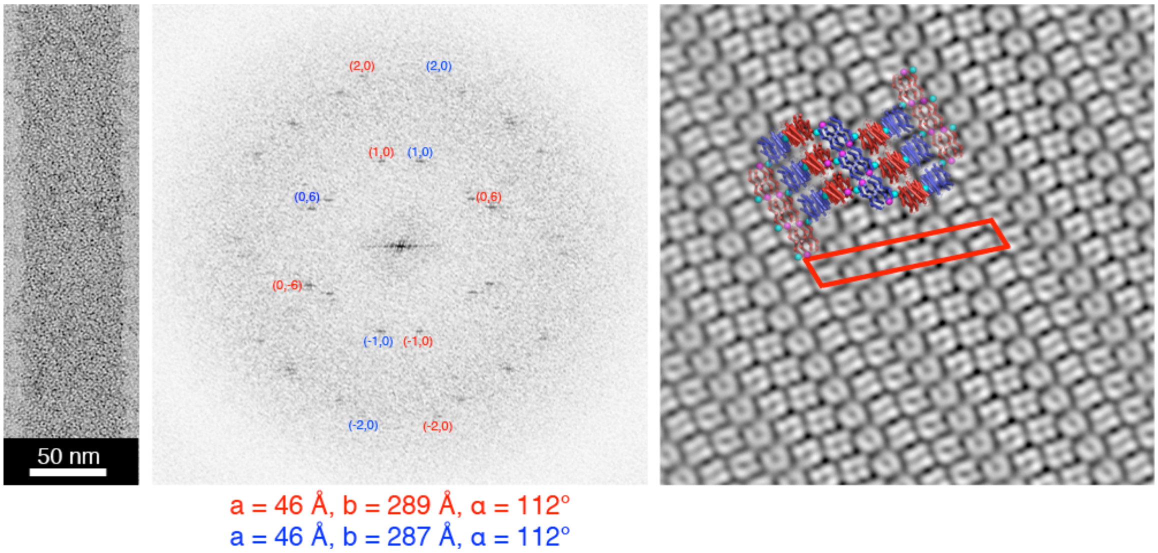

Figure S12. TEM image of a single nanotube (left), indexed Fourier transform (center), and 2D reconstructions (right) of a Class III nanotube.

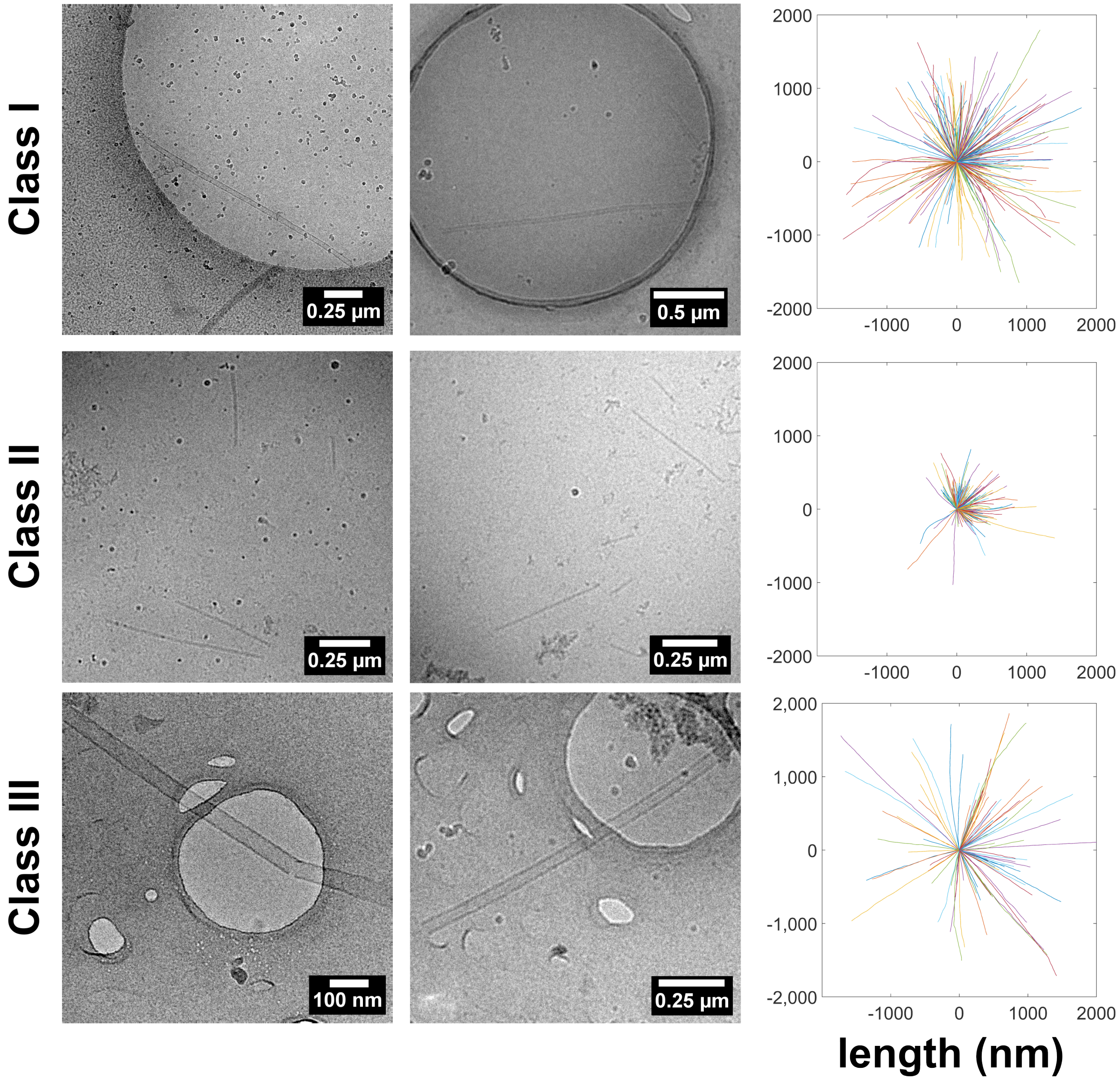

Figure S13. Representative images of nanotubes collected by cryo TEM. The plots on the right show the tracing of each nanotube starting from position (0,0). Axes are in nanometers.

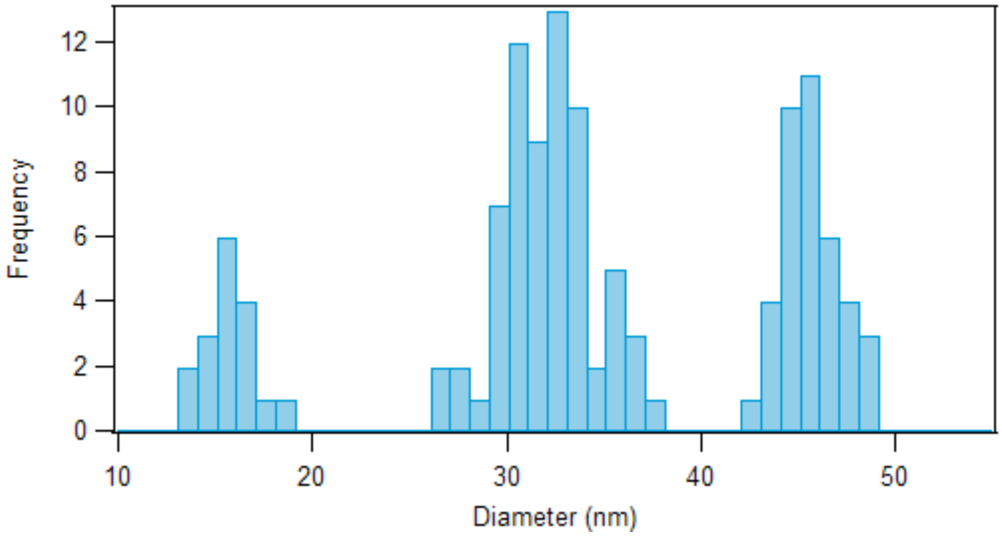

Figure S14. Width distribution of tubes as measured in cryoEM samples.

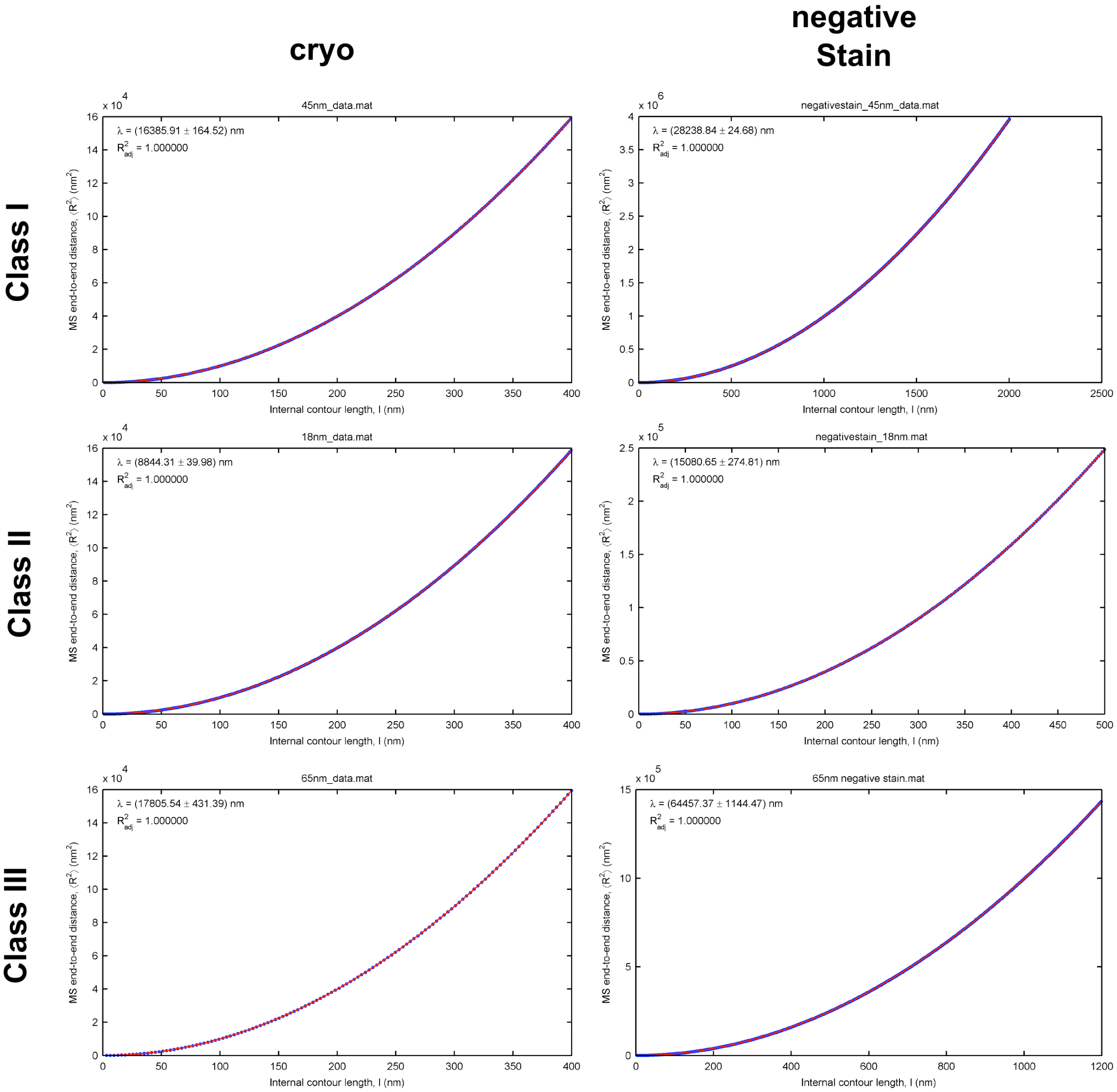

Figure S15. Fits used for calculating persistence length using the FiberApp module "MS End-to-end Distance". Please refer to the corresponding section in Materials and Methods for details.

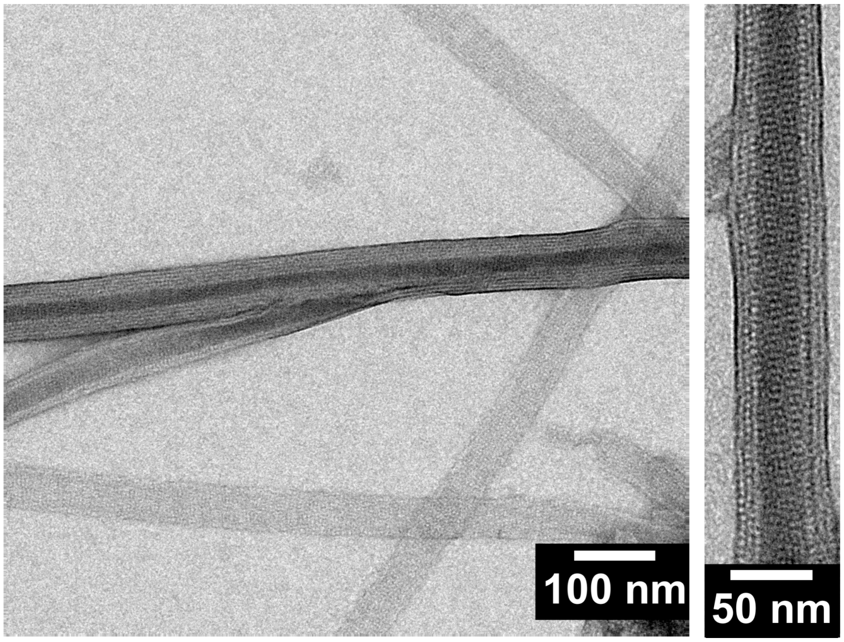

Figure S16. TEM micrograph of multi-walled tubes formed under conditions that also produce Class I tubes.

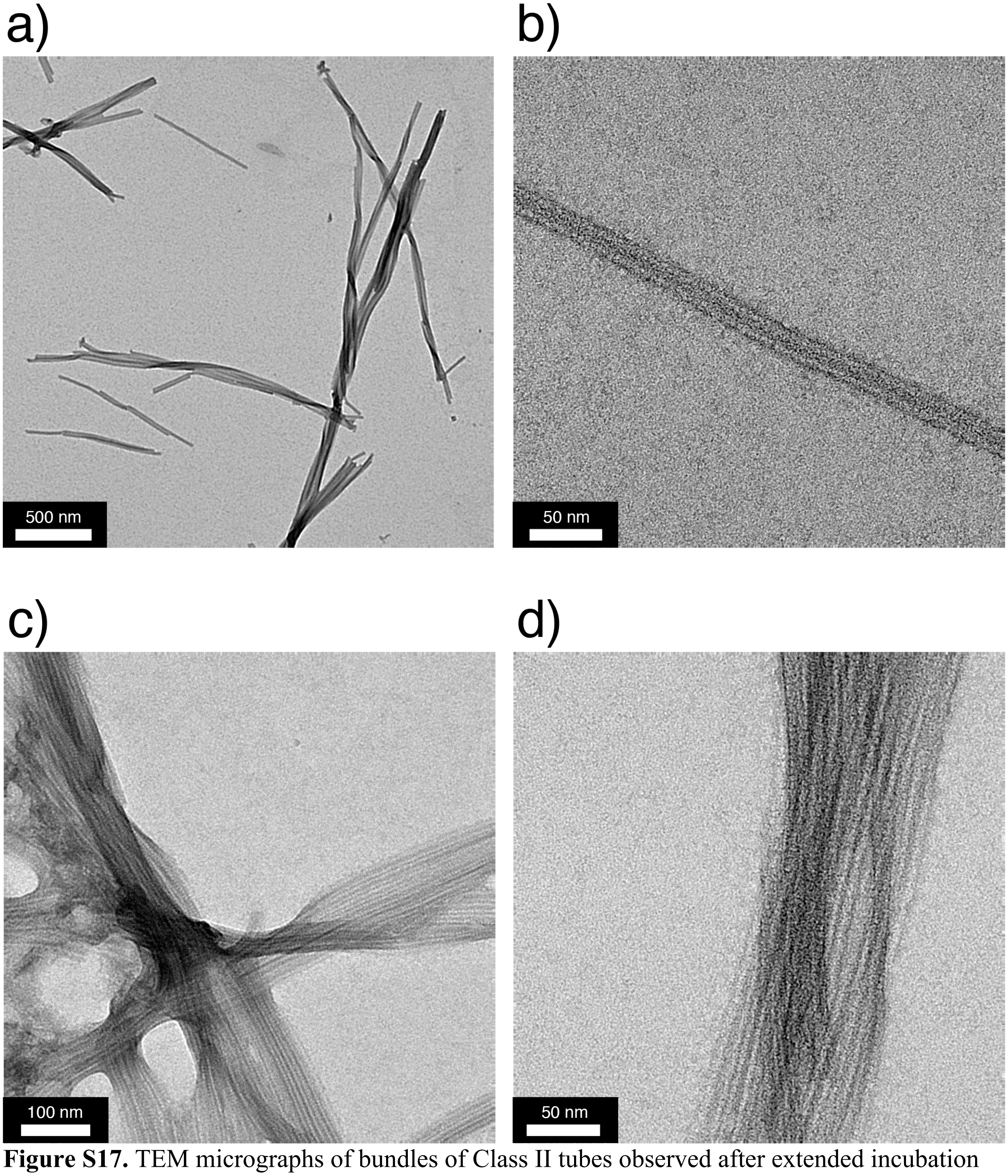

Figure S17. TEM micrographs of bundles of Class II tubes observed after extended incubation periods.

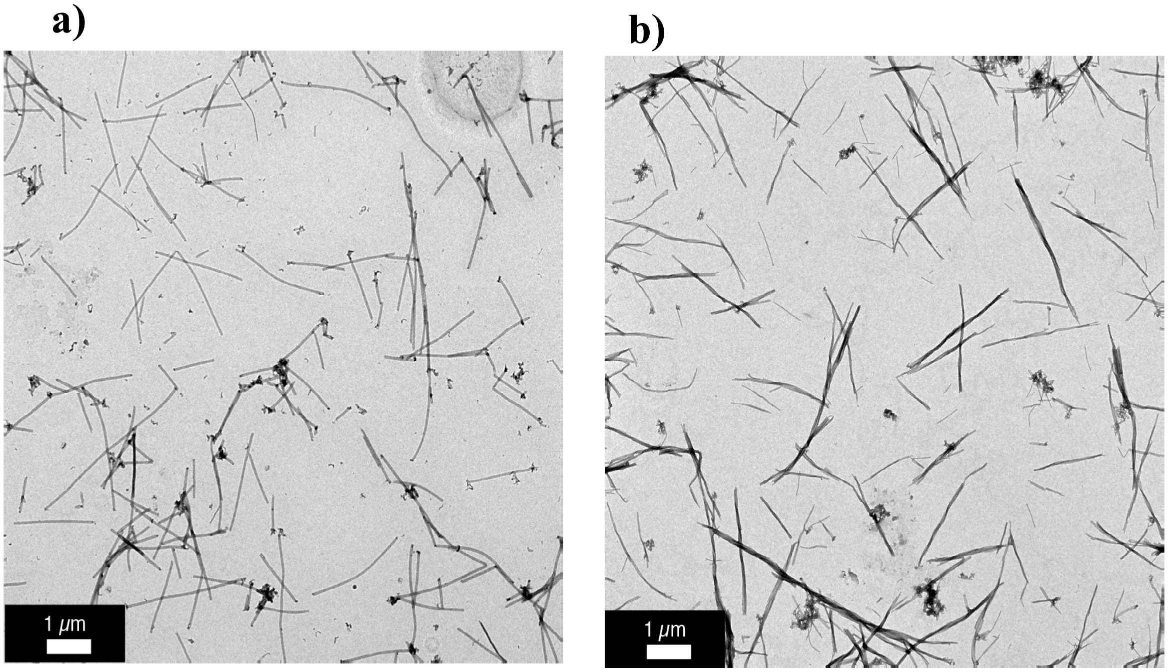

Figure S18. Low magnification TEM micrographs of class I (a) and class II (b) nanotubes after incubation for 1 year at room temperature.

Supporting References:

(1) Brodin, J. D.; Ambroggio, X. I.; Tang, C.; Parent, K. N.; Baker, T. S.; Tezcan, F. A. *Nat. Chem.* **2012**, *4*, 375.
(2) Salgado, E. N.; Faraone-Mennella, J.; Tezcan, F. A. *J. Am. Chem. Soc.* **2007**, *129*, 13374.
(3) Winn, M. D.; Ballard, C. C.; Cowtan, K. D.; Dodson, E. J.; Emsley, P.; Evans, P. R.; Keegan, R. M.; Krissinel, E. B.; Leslie, A. G. W.; McCoy, A.; McNicholas, S. J.; Murshudov, G. N.; Pannu, N. S.; Potterton, E. A.; Powell, H. R.; Read, R. J.; Vagin, A.; Wilson, K. S. *Acta Crystallogr. D* **2011**, *67*, 235.
(4) Mccoy, A. J.; Grosse-Kunstleve, R. W.; Adams, P. D.; Winn, M. D.; Storoni, L. C.; Read, R. J. *J. Appl. Crystallogr.* **2007**, *40*, 658.
(5) Murshudov, G.; Vagin, A.; Dodson, E. *Acta Cryst.* **1996**, *D53*, 240.
(6) Emsley, P.; Cowtan, K. *Acta Crystallogr. D* **2004**, *D60*, 2126.
(7) DeLano, W. L. *The PYMOL Molecular Graphics System (http://www.pymol.org)*, 2003.
(8) Gipson, B.; Zeng, X.; Zhang, Z. Y.; Stahlberg, H. *J. Struct. Biol.* **2007**, *157*, 64.
(9) Usov, I.; Mezzenga, R. *Macromolecules* **2015**, *48*, 1269.